

DOI: 10.1002/adem.201400151

Electrospray Deposition of Energetic Polymer Nanocomposites with High Mass Particle Loadings: A Prelude to 3D Printing of Rocket Motors**

By Chuan Huang, Guoqiang Jian, Jeffery B. DeLisio, Haiyang Wang and Michael R. Zachariah*

One of the challenges in the use of energetic nanoparticles within a polymer matrix is the difficulty in processing by traditional mixing methods. In this paper, electrospray deposition is employed to create high loadings of aluminum nanoparticles (Al-NPs) in polyvinylidene fluoride (PVDF) reactive composite films. The deposited films containing up to 50 wt% Al are found to be crack free and mechanically flexible. Thermochemical behavior characterized by thermogravimetric (TG) and differential scanning calorimetry (DSC) analysis shows that the addition of Al-NPs sharply reduces the onset decomposition temperature due to a pre-ignition reaction occurring in the film. The combustion propagation velocity in air at three different mass loading of Al-NPs shows burning rates of 5, 16, and 23 cm s⁻¹ for loadings of 16.7, 30, and 50 wt% Al-NPs. The results suggest electrospray deposition as a direct approach to make bulk polymer composites containing high metal particle mass loading and may be a prelude to 3D printing of rocket motors.

1. Introduction

Polymer composites containing reactive metal (e.g., aluminum) are of extreme importance in propellants, such as solid rocket motors used in the Space Shuttle.^[1,2] Ideally, the purpose of the polymer is to give the fuel mechanical integrity, but should also participate in a favorable manner in the overall energy release chemistry.^[3,4] A variety of binders have been employed including epoxy-, nitrocellulose-, and fluorine-containing polymers.^[5-7] In the latter case, fluorine-containing binders offer a delivery method for a very strong oxidizer.^[8]

During the last decade, nano-size aluminum (n-Al) has received increased interest due to its greatly increased burning rate, as compared to its micron-sized counterpart.^[9-14] The prevailing wisdom is that n-Al enhanced reactivity is primarily related to its increased specific surface area. However, while nanoscale reactive components offer high potential game changing performance, fabricating polymer formulations with high mass loading of these reactive components has proved to be very challenging. In part, this is due to the rapid increase in viscosity of the polymer melt upon addition of high surface area nanomaterials that makes casting virtually impossible.^[15,16] In this study, we demonstrate the ability to employ electrospray deposition to create high mass loadings of nanoaluminum in polymeric films. The use of this approach is a prelude to what might evolve into a 3D printing approach for propellants.

As we noted above, fluoropolymers as an oxidizer of aluminum have attracted considerable interest due to the strong oxidation potential of fluorine and the high heat of reaction to form aluminum fluoride (AlF₃).^[3] The metric of note is that formation of AlF₃ relative to alumina releases about 80% more energy per unit mass than oxidation of aluminum (55.7 and 31 kJ g⁻¹, respectively).^[17] In addition, some fluoropolymers have been used to functionalize or add additional passivation layers on n-Al, so as to prevent the further oxidation of the core.^[18-21] An important class of fluoropolymers is polyvinylidene fluoride (PVDF), which contains 59.4% fluorine by mass, has high mechanical strength, excellent thermal stability, and chemical resistance,

[*] Prof. M. R. Zachariah, C. Huang, Dr. G. Jian, J. B. DeLisio, H. Wang

Department of Chemical and Biomolecular Engineering, University of Maryland, College Park, Maryland 20742, USA
Department of Chemistry and Biochemistry, University of Maryland, College Park, Maryland 20742, USA
E-mail: mrz@umd.edu

[**] This work was financially supported by the Defense Threat Reduction Agency and the Army Research Office. We acknowledge the support of the Maryland Nanocenter and its NispLab. The NispLab is supported in part by the NSF as a MRSEC Shared Experimental Facility. The authors also acknowledge Dr. Sandip Haldar for the micromechanical test and Philip Michael Guerieri for helping build the combustion chamber. Supporting Information is available from the Wiley Online Library or from the author.

and has been widely used as a binder.^[22] This polymer can be dissolved in some polar solvents such as acetone, dimethylformamide (DMF), and dimethyl sulfoxide and is commercially available at relatively low cost compared to other fluoropolymers. Here, we have introduced it as the oxidizer and/or reactive binder for aluminum.

Electrostatic spray deposition (ESD) has been considered as an effective means for the deposition of nano or micro films.^[23–26] In the ESD process, an electrically conducting liquid solution is charged when it flows through a fine nozzle connected to high voltage. Charge that builds up on the fluid surface creates a columbic driven hydrodynamic instability that overcomes the surface tension of the solution, resulting in the formation of small, charged monodisperse droplets. In our case, these fine droplets are subsequently deposited onto a substrate to form uniform solid films following solvent evaporation. Both polymer and inorganic films have been fabricated by this method.^[27–31] ESD offers several advantages. First, it can conveniently control the thickness, morphology, and uniformity of film by adjusting the solution concentration, flow rate, and applied voltage. Second, the apparatus used in the method are simple and cheap. Finally, it can be performed at ambient temperature under atmosphere pressure.

Previously, we have reported the electrospinning of thermite-based nanofiber mats, and the electro spray production of nanoaluminum microspheres.^[6,32] In this work, electro spray is extended to fabricate Al/PVDF energetic films with high mass loading of nanoparticles (up to 50 wt%). We find that adding a small quantity of ammonium perchlorate (AP) salt in the precursor significantly improved the morphology of the as-prepared free-standing film. The resulting nanocomposite film shows good mechanical integrity. Combustion behavior in air showed that propagation rates are closely correlated to the Al content in the films. To the best of our knowledge, the electro spray deposition technique has not previously been applied to fabricate energetic composite films.

2. Experimental

2.1. Materials

Aluminum nanopowders (Al-NPs) (ALEX, 50 nm) used in this work were purchased from Argonide Corporation. The active Al was 70% by mass determined by thermogravimetric analysis (TGA). PVDF (Mw = 534,000) (PVDF), DMF (99.8 wt %), and AP (99.8 wt%) purchased from Sigma–Aldrich were directly used as received.

2.2. Precursor Preparation

In a typical experiment, 100 mg mixtures of Al-NPs and PVDF powders (the content of Al-NPs in mixtures is 16.7, 30, and 50% by weight, respectively. Among these three different mass ratio, the 30 wt% Al-NPs content is closest to unity stoichiometric ratio, which is 31.4 wt%) and an additional 2 mg of ammonium perchlorate (AP) were dissolved in 1 mL DMF solvent. The mixture was first vigorously stirred for 2 h and then sonicated for 1 h, followed by 24 h magnetic stirring.

2.3. Electro spray Deposition

The experiment system is schematically shown in Figure 1a. The dual spray system includes two syringe pumps operating with a feed rate of 1.5 mL h⁻¹ connected to stainless steel needles (23 gauge, inner diameter: 0.43 mm; outer diameter: 0.63 mm). The two needles connected by a copper wire (1 mm) are 1 cm apart and positioned 5 cm from the rotating drum substrate, with an electric field of 4 kV cm⁻¹ (a 10 kV positive voltage applied on the needles and a 10 negative voltage applied on the substrate).

2.4. Characterization

The mechanical properties of as-prepared nanocomposite films were tested by a custom-built microtensile tester using dog-bone specimens with gauge lengths ≈5 mm and widths ≈1 mm. Three samples were tested for each film at a quasi-static loading strain rate of 10⁻⁴ s⁻¹ controlled by customized picomotor control software with a less than 25 N load cell. Strain in the gage section of the specimen was obtained by a video extensometer comprising of a Point Grey Flea2 (FL2-14S3C) digital camera and a stereo microscope.^[33] The stress is given by the ratio of force measurement from the load cell to the initial measurement thickness and width of the sample gauge section.

The surface morphologies and thickness of the film were characterized using a scanning electron microscope (SEM; Hitachi, SU70 FEG-SEM) equipped with energy dispersive X-ray spectroscopy (EDS). Before being tested, all samples were sputtered with carbon. For cross-sectional SEM images, samples were first fractured in liquid nitrogen and then sputtered with carbon.

Thermogravimetric (TG) and differential scanning calorimetry (DSC) analysis were performed on a SDT Q600 (TA instruments) under flowing nitrogen (50 mL min⁻¹). Two to

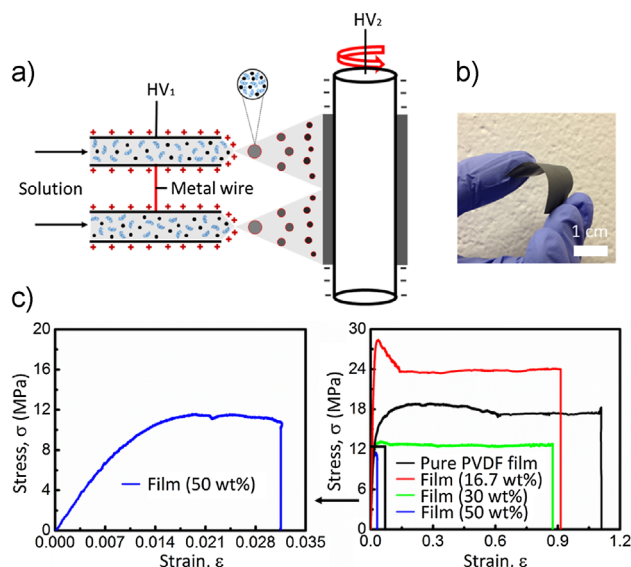


Fig. 1. (a) Electro spray deposition of Al/PVDF film, (b) photograph of a free-standing film with 50 wt% nanoaluminum loading, (c) stress–strain curves of nanocomposite films containing between 0 and 50 wt% nanoaluminum by electro spray deposition.

three milligrams of samples were placed into an alumina pan and heated from room temperature up to 900 °C at a rate of 20 °C min⁻¹.

The combustion behavior of the films was captured using a high-speed camera (Plantom v 12.0) with a frame rate of 7000 frames per second in both air and argon environments. Basically, a 4 cm long and 1 cm wide film is fixed on two glass slides that is 0.9 cm apart, and fixed on a ceramic stage (shown in Supporting Information Figure S1). For an open air test, a 4 cm long and 1 cm wide film was ignited by the flame of a trigger igniter (Bernzomatic). The combustion of Al/PVDF film in ambient argon was performed in a homemade chamber filled with argon and ignited by resistively heating a nichrome wire triggered by an external DC power supply. PCC 1.2 software (Phantom, Inc.) was used to analyze the images from the camera and calculate the burning rate of the Al/PVDF film.

Post-combustion products were characterized by powder X-ray diffraction (XRD; Bruker C2 Discover with GADDS, operating at 40 kV and 40 mA with unfiltered Cu Ka radiation, $E = 8049$ eV, $k = 1.5406$ Å).

3. Results and Discussion

Figure 1a shows a schematic diagram of the electrospray method used in this experiment. Two spray systems were used to deposit a uniform and thick film. The thickness and morphology of the electrosprayed film can be controlled easily by the physical properties of solution and process parameters. Figure 1b shows a photograph of a 50 wt% Al/PVDF free-standing film that was easily lifted off from the substrate indicating the material has substantial mechanical integrity.

3.1. Physical Characteristics

The density of the electrosprayed films was determined by a mass and volume measurement (calculated from its thickness and area), and the porosity of film was estimated using:

$$\text{Porosity} = 1 - \frac{\rho_{\text{measurement}}}{\rho_{\text{theoretical}}} \quad (1)$$

Here, the density of PVDF and nanoaluminum was taken as 1.74 and 2.7 g cm⁻³ (supplier information), respectively. The density and porosity of as-prepared films are summarized in Table 1. These results indicate that porosity increases as the wt % of Al-NPs is increased, and from 4.3 to 27.4%.

As reported in various references,^[34–38] adding a small quantity of nanostructured materials such as nanoparticles, nanosheets, and nanotubes into a polymer matrix, can improve the mechanical properties of nanocomposites, via the formation of a co-network between the nanomaterial and polymer chain. However, higher loadings result in agglomeration and leads to poor mechanical properties.^[37,38] In our case, a similar result is observed, and shown in Figure 1c and

Table 1. Density and porosity of electrospray films.

	Pure PVDF film	16.7 wt% film	30 wt% film	50 wt% film
Density [g cm ⁻³]	1.64	1.77	1.63	1.54
Porosity [%]	5.70	4.30	16.4	27.4

Note: 16.7, 30, and 50 wt% film corresponds to film loading of 16.7, 30, and 50 wt% Al-NPs.

Supporting Information Table S1. The addition of Al-NPs with low mass loading slightly increases the tensile strength from 18 MPa at 0 wt% to 24 MPa at 16.7 wt%, however, upon further increase in Al-NP loading, the tensile strength decreases. This is especially true for the high mass loading (50 wt%) sample where the tensile strength decreases to 11 Mpa. Similarly, the toughness slightly increases from 19 MJ m⁻³ at 0 wt% to 22 MJ m⁻³ at 16.7 wt% particle loading, then dramatically decreases to 0.28 MJ m⁻³ at 50 wt% particle loading. The Young's modulus increases when adding the nanoparticles from 640 MPa at 0 wt% to 1300 MPa at 16.7 wt% particle loading and then drops to 850 MPa at 50 wt% particle loading. In addition, adding Al-NPs also influences strain. Despite the loss of mechanical properties, the nanocomposite films containing 50 wt% nanoparticles, as illustrated in Figure 1b, are non-brittle, and can be deformed and flexed.

Empirically, we found that to create a crack-free film, a small quantity of soluble inorganic salt was needed (AP) to decrease the droplet size in the electrospray through the scaling law: Droplet diameter $\approx K^{-0.33}$, where K is the solution electrical conductivity.^[26] Here, the AP serves a dual function of improving film morphology, but also has an oxidative potential. However, at our loadings (<2%) it is unlikely to have much of a combustion effect. Figure 2a and b shows the typical SEM top-view images of films deposited with the added AP in the suspension. The low magnification image shows a film that is crack-free and smooth, but also exhibits some irregularity. Particles are coated and/or connected by polymer, as shown in Figure 2b, and the similarity is also observed at 16.7 and 30 wt%, respectively (Supporting Information Figure S2). Particles are also dispersed in the polymer matrix, although some aggregation is also taking place (Supporting Information Figure S3). In the absence of AP, the deposited material cannot be peeled off from the substrate to form a whole film, and SEM imaging showed the film was inhomogeneous with considerable porosity (Supporting Information Figure S4). Thus, decreasing drop diameter appears to enable formation of a free-standing film. The cross-sections for imaging (Figure 2c and d) were obtained by immersion and fracture in liquid nitrogen. The films are uniform thickness (about 170 μm) with what appear to be some fibrous polymer network. It is clear that some inhomogeneity is apparent, in which we see some aggregation of the nanoparticles. This probably is what is responsible for

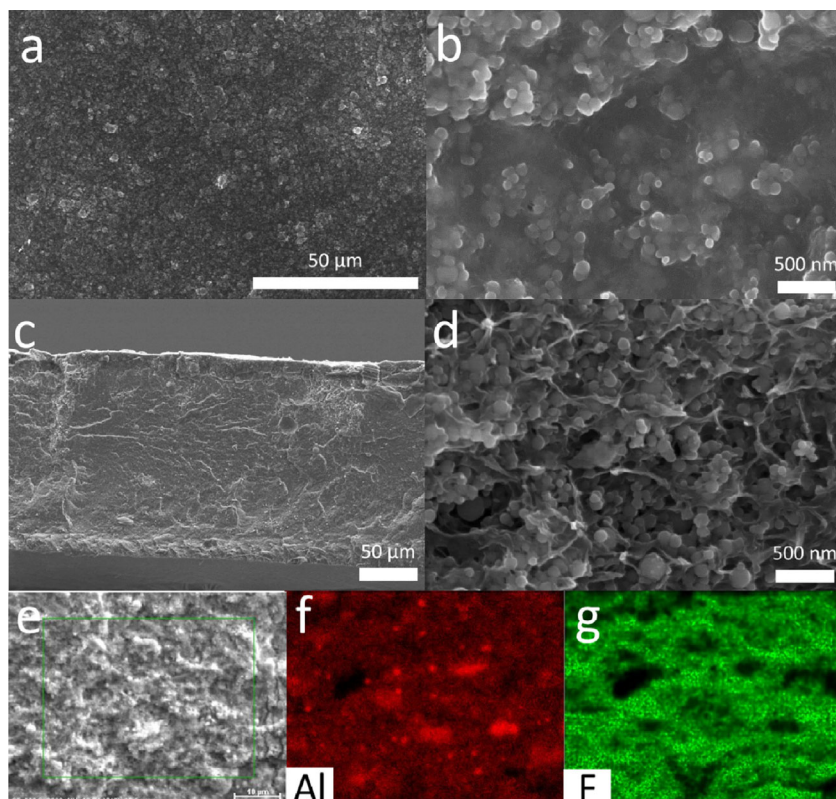


Fig. 2. SEM images of films deposited by electro spray with 50 wt% Al-NPs loading and adding AP. (a) Top-view of the film's surface; (b) close-up of the top-view; (c) cross-section of film; (d) close-up of cross section. Elemental mapping analysis of cross-section of film with 50 wt% Al-NPs loading (e-g).

the elevated porosity observed at the higher particle loadings, and the corresponding loss of mechanical strength.

One of the primary goals of this study was to demonstrate that NP's could be incorporated within a polymer matrix at high loadings (50 wt%) to form free-standing film, potentially as a prelude to forming a 3D structure. Figure 3 shows the limit to which the current approach can be applied for films with up to 65 wt% NP's. In this case, the electro spray materials morphology becomes the microparticles, rather than free-standing film. This is similar to what we have observed in the formation of gelled Al microspheres.^[32]

3.2. Thermal and Reactive Properties

TG and DSC analysis was performed in nitrogen to evaluate thermal stability and reactivity, following vacuum heating at 70 °C for 12 h to remove any residual solvent. TGA of pure PVDF and three different Al mass loading films are shown in Figure 4a. The pure PVDF shows a sharp mass loss at 410 °C, with a residual mass of 23%, implying mostly high volatility products.

As reported by Zulfiqar *et al.*^[39] the main decomposition product of PVDF is hydrogen fluoride (HF), which agrees with our observed mass loss. In contrast, the TGA curves of three nanocomposite films under the same conditions shows several distinct mass losses, the first at 190 °C, the second at 340 °C, and for the high particle mass loading film, there is a third step yielding at 400 °C. The total weight loss of the low,

moderate, and high particle mass loading films are 50, 39, and 23%, respectively. These values are significantly less than the weight loss, if just considering the polymer decomposition with no impact from the nanoaluminum in nanocomposite films, which could be 64.5, 53.9, and 38.5%, respectively. That indicates the nanoaluminum reacts with the gas product of the decomposition of PVDF or polymer matrix, which results in decreasing the amount of volatility products. DSC analysis (Figure 4b), shows an initial endotherm at 140–170 °C (magnified image shown in Figure 4c), is associated with polymer melting,^[40] and the subsequent two exotherms correspond to the mass loss observed in the TGA curves. In addition, the final endotherm in the high particle loading film at temperature range of 640–670 °C should be associated with the melting (m. p. = 633 °C) of unreacted aluminum.^[41] The first small exotherm at the range of 190–300 °C (the magnified image shown in Figure 4d) indicates a pre-ignition reaction in the nanocomposite films (a similar exotherm for the reaction of nanoaluminum + Teflon).^[42] In comparison to the reaction between aluminum and Teflon, the pre-ignition reaction is still observed in Al/PVDF composite films, although PVDF contains hydrogen in addition to carbon and fluorine. This indicates that the hydrogen on the PVDF chain does not hinder the pre-ignition from occurring. One major result is that the addition of Al-NPs promotes the decomposition of the polymer, despite the fact that this occurs well below the aluminum melting point. This implies that melting of the polymer enables reaction of fluorine with the alumina shell in the Al-NP's to generate AlF₃ and accelerate the decomposition of the polymer.^[42,43]

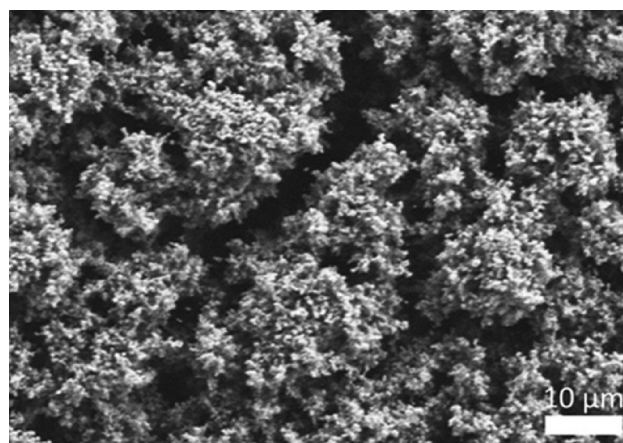


Fig. 3. SEM surface morphology image of Al/PVDF film with 65% Al-NPs, shows the limit to which NP's can be added.

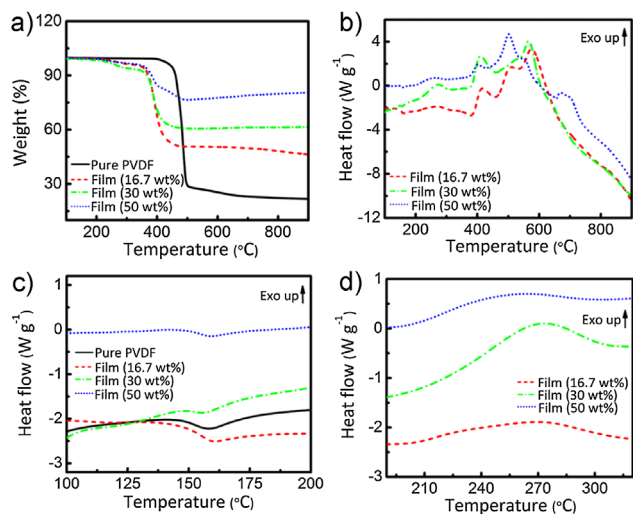


Fig. 4. Thermal analysis ($20\text{ }^{\circ}\text{C min}^{-1}$) of pure PVDF and as-prepared Al/PVDF film under the nitrogen flow. (a) The thermogravimetry curve; (b–d) the differential scanning calorimetry curve. Note: the wt% given in the parentheses means the mass loading of Al-NPs in the film.

We now turn our attention to the combustion properties of the Al/PVDF energetic films. The combustion propagation velocity was measured by igniting a 4 cm length by 1 cm width film. For each sample, three experiments were run to calculate the average combustion propagation velocity. As a comparison, films were ignited in both air and argon environment. Figure 5a shows a representative flame propagation schematic of Al/PVDF film. Figure 5b–d shows high speed imaging of the burning processes of Al/PVDF films with different Al-NP loadings in air and argon environments. All the films were easily ignited and demonstrated a self-sustaining steady propagating combustion, as shown in Figure 5. Figure 6 shows the average combustion propagation velocities of Al/PVDF films in air and argon, respectively. For films burning in argon, the flame propagation velocity is significantly lower than burning in air at the same Al nanoparticle mass loading except for low particle mass loading film (16.7 wt%), which has almost the same burn speed in both experimental conditions. The combustion of moderate particle loading film (30 wt% Al) had the highest velocity (11 cm s^{-1}). This mass loading of aluminum corresponds to the stoichiometric mixture, which will be discussed later on. In comparison, when burning in air, the highest velocity (23 cm s^{-1}) appeared at the highest particle loading (50 wt%) Al/PVDF film.

In comparison to previously reported similar energetic films, which were a spray-coated blend of nanoaluminum and THV-220A (a class of fluoropolymer oxidizer) dispersed in acetone on substrates, burn rates up to 1.3 m s^{-1} were observed.^[44] The free-standing film in this work shows low burn rate (subsonic burn speed $<1\text{ m s}^{-1}$).^[3] Interestingly, the Al/PVDF nanocomposite films have the same order of burn rate as previously reported pressed Al/Teflon nanocompo-

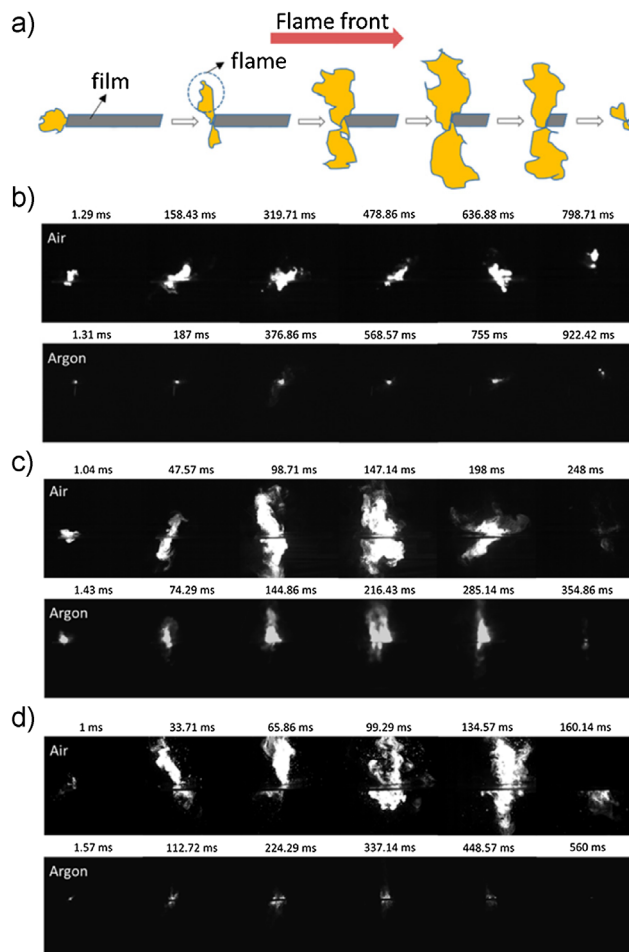


Fig. 5. (a) Schematic showing of flame propagation. (b–d) Selected frames of Al/PVDF films combustion using high speed camera, with loading 16.7, 30, and 50 wt% Al-NPs, respectively. Note: The time stamps on the top of each picture indicated elapsed time from the starting trigger.

sites (several cm s^{-1}) while the spray-coated films have the same order of burn rate as the nanoaluminum/Teflon loose powders under an open burn test (up to 4.5 m s^{-1}).^[45,46] The latter two nanocomposites were involved in half-confined combustion and had a loose structure. This has a positive effect on the burn rate,^[46–48] which can explain these higher burn rates when compared to the Al/PVDF films and pressed Al/Teflon nanocomposite. The lower burn rate of the Al/PVDF film may not be a disadvantage because of its primary intended use as a propellant.

In air, combustion of Al/PVDF films showed very high luminosity, and increased flame speed, which increased with Al-NPs content in the film, as shown in Figure 5b–d and 6, respectively. Evaluation of the residue by XRD shown in Figure 7, indicates the primary crystalline phase of Al_2O_3 is seen in all three samples, though only weakly for the low 16.7 wt% Al content case. Al_4C_3 was found only in the residue at high Al particle loadings, but surprisingly, no AlF_3 was observed. The latter case may be attributed to the low boiling point of AlF_3 (b.p. = $1277\text{ }^{\circ}\text{C}$).

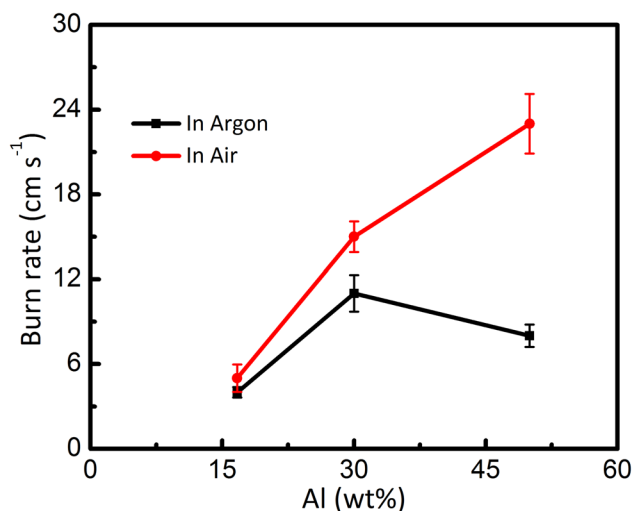


Fig. 6. Combustion propagation velocity of Al/PVDF films as a function of particle mass loading in air and argon.

In contrast, the combustion of same particle loading films in argon is less intense than in air (Figure 5b–d), and the combustion of low Al-NPs loading film yielded a weak visible flame. A large amount of solid residue and smoke were produced. XRD analysis shows that the primary component in all solid residues is AlF₃. Crystalline elemental Al was also observed in the high particle loading film, indicating an incomplete combustion in argon, which is

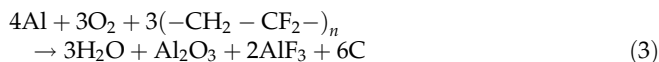
consistent with the DSC analysis of high particle loading film shown in Figure 4b.

Considering the main decomposition product of PVDF is HF, we postulate the net reaction between aluminum and PVDF proceeds as follows



The stoichiometric reaction of aluminum and PVDF producing hydrogen, AlF₃ and carbon (in Equation 2) requires 22% Al and 78% PVDF by weight. The Al-NPs used in this experiment are 70 wt% active aluminum due to the presence of oxide shell that contributes nothing to the reaction.^[49] Considering that fact, the reasonable composition equivalent is 31.4 wt% Al-NPs and 68.6 wt% PVDF. The 30 wt% Al-NPs film is the closest to the stoichiometric composition in the three mass ratio films, and it shows the fastest combustion propagation velocity in argon ambient (Figure 6).

In the open air burning tests, oxygen is involved in the combustion process (the XRD patterns shows there is significant Al₂O₃ in the residue), thus both the fluorination and oxidation contribute to the reaction. Consequently, Equation 2 can be converted to Equation 3



The composition equivalent obtained from Equation 3 is 51.4% Al-NPs and 48.6% PVDF by weight. In these experiments, the tested 50 wt% Al-NPs film is very close to this ratio and was consumed in the shortest overall time.

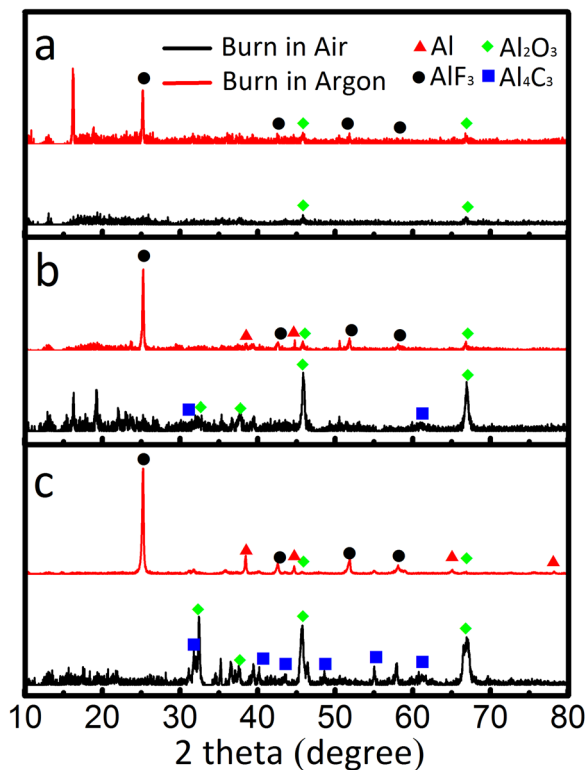


Fig. 7. XRD patterns of solid residue of Al/PVDF films after burning in air and argon, Al content in: (a) 16.7 wt% Al-NPs; (b) 30 wt% Al-NPs; (c) 50 wt% Al-NPs.

4. Conclusion

In summary, we have demonstrated that electrospray deposition of metal particle–polymer suspensions can be used as a novel and simple method for fabrication of metal-based energetic composites. We demonstrate the ability to form crack free, free-standing films with mechanical integrity containing up to 50 wt% nanoparticles of aluminum that are homogeneously dispersed within the polymer matrix. Thermal analysis reveals that integrating the Al-NPs into the polymer matrix decreased the onset decomposition temperature and their pre-ignition reaction in the films. The films demonstrated steady self-propagating combustion, which was optically intense and strongly correlated with the amount of aluminum loading, with the highest loading showing the fastest propagation speed in air.

Received: March 28, 2014

Revised: May 27, 2014

Published online: August 28, 2014

- [1] E. Diaz, *Prop. Explos. Pyrotech.* **2003**, *28*, 210.
- [2] X. Zhang, W. M. Hikal, Y. Zhang, S. K. Bhattacharia, L. Li, S. Panditrao, S. Wang, B. L. Weeks, *Appl. Phys. Lett.* **2013**, *102*, 141905.

- [3] E. C. Koch, *Metal-Fluorocarbon Based Energetic Materials*, Wiley-VCH Verlag GmbH & Co. KGaA, Weinheim, Germany **2012**.
- [4] H. A. Miller, B. S. Kusel, S. T. Danilson, J. W. Neat, E. K. Avjian, S. N. Pierson, S. M. Budy, D. W. Ball, S. T. Iacono, S. C. Kettwich, *J. Mater. Chem. A* **2013**, *1*, 7050.
- [5] R. A. Austin, D. L. McDowell, D. J. Benson, *Modell. Simul. Mater. Sci. Eng.* **2006**, *14*, 537.
- [6] S. Yan, G. Q. Jian, M. R. Zachariah, *ACS Appl. Mater. Interf.* **2012**, *12*, 6432.
- [7] R. H. B. Bouma, D. Meuken, R. Verbeek, M. M. Pacheco, L. Katgerman, *Prop. Explos. Pyrotech.* **2007**, *32*, 447.
- [8] S. C. Stacy, M. L. Pantoya, D. L. Prentice, E. D. Steffler, M. A. Daniels, *Adv. Mater. Process.* **2009**, *107*, 33.
- [9] R. A. Yetter, G. A. Risha, S. F. Son, *Proc. Combust. Inst.* **2009**, *32*, 1819.
- [10] E. L. Dreizin, *Prog. Energy Combust.* **2009**, *35*, 141.
- [11] M. L. Pantoya, J. J. Granier, *Prop. Explos. Pyrotech.* **2005**, *30*, 53.
- [12] G. Q. Jian, J. Y. Feng, R. J. Jacob, G. C. Egan, M. R. Zachariah, *Angew. Chem. Int. Ed.* **2013**, *52*, 9743.
- [13] B. S. Bockmon, M. L. Pantoya, S. F. Son, B. W. Asay, J. T. Mang, *J. Appl. Phys.* **2005**, *98*, 064903.
- [14] J. A. Puszynski, C. J. Bulian, J. J. Swiatkiewicz, *J. Propul. Power* **2007**, *23*, 698.
- [15] L. Meda, G. Marra, L. Galfetti, S. Inchingalo, F. Severini, L. D. Luca, *Compos. Sci. Technol.* **2005**, *65*, 769.
- [16] L. Galfetti, L. T. D. Luca, F. Severini, L. Meda, G. Marra, M. Marchetti, M. Regi, S. Bellucci, *J. Phys.: Condens. Matter* **2006**, *18*, S1991.
- [17] D. R. Lide, *77th CRC Handbook of Chemistry and Physics*, CRC Press, Boca Raton, Florida **1996**.
- [18] R. J. Jouet, A. D. Warren, D. M. Rosenberg, V. J. Bellitto, K. Park, M. R. Zachariah, *Chem. Mater.* **2005**, *17*, 2987.
- [19] K. S. Kappagantula, C. Farley, M. L. Pantoya, J. Horn, *J. Phys. Chem. C* **2012**, *116*, 24469.
- [20] B. Dikici, S. W. Dean, M. L. Pantoya, V. I. Levitas, R. J. Jouet, *Energy Fuels* **2009**, *23*, 4231.
- [21] D. Kaplowitz, G. Q. Jian, K. Gaskell, A. Ponce, P. J. Shang, M. R. Zachariah, *Part. Part. Syst. Charact.* **2013**, *30*, 881.
- [22] Y. Wang, S. J. Travas, R. Steiner, *Solid State Ionics* **2002**, *148*, 443.
- [23] A. Jaworek, *J. Mater. Sci.* **2007**, *42*, 266.
- [24] J. H. Kim, K. W. Nam, S. B. Ma, K. B. Kim, *Carbon* **2006**, *44*, 1963.
- [25] I. B. Rietveld, N. Sukanuma, K. Kobayashi, H. Yamada, K. Matsushige, *Macromol. Mater. Eng.* **2008**, *293*, 387.
- [26] I. B. Rietveld, K. Kobayashi, H. Yamada, K. Matsushige, *J. Colloid Interface Sci.* **2009**, *339*, 481.
- [27] B. Hoyer, G. Sorensen, N. Jensen, D. B. Nielsen, B. Larsen, *Anal. Chem.* **1996**, *68*, 3840.
- [28] V. N. Morozov, T. Y. Morozova, N. R. Kallenbach, *Int. J. Mass Spectrom.* **1998**, *178*, 143.
- [29] Y. Yu, C. H. Chen, Y. A. Shi, *Adv. Mater.* **2007**, *19*, 993.
- [30] C. H. Chen, E. M. Kelder, P. J. J. M. van der Put, J. Schoonman, *J. Mater. Chem.* **1996**, *6*, 765.
- [31] Y. Z. Zhang, L. H. Wu, E. Q. Xie, H. G. Duan, W. H. Han, J. G. Zhao, *J. Power Sources* **2009**, *189*, 1256.
- [32] H. Y. Wang, G. Q. Jian, S. Yan, J. B. DeLisio, C. Huang, M. R. Zachariah, *ACS Appl. Mater. Interfaces* **2013**, *5*, 6797.
- [33] A. L. Gershon, D. P. Cole, A. K. Kota, H. A. Bruck, *J. Mater. Sci.* **2010**, *45*, 6353.
- [34] A. Bansal, H. C. Yang, C. Z. Li, K. L. Cho, B. C. Benicewicz, S. K. Kumar, L. S. Schadler, *Nat. Mater.* **2005**, *4*, 693.
- [35] D. Maillard, S. K. Kumar, B. Fragneaud, J. W. Kysar, A. Rungta, B. C. Benicewicz, H. Deng, L. C. Brinson, J. F. Douglas, *Nano Lett.* **2012**, *12*, 3909.
- [36] T. Ramanathan, A. A. Abdala, S. Stankovich, D. A. Dikin, M. H. Alonso, R. D. Piner, D. H. Adamson, H. C. Schniepp, X. Chen, R. S. Rouff, S. T. Nguyen, I. A. Aksay, R. K. Prudhomme, L. C. Brinson, *Nat. Nanotechnol.* **2008**, *3*, 327.
- [37] T. Sekitani, Y. Noguchi, K. Hata, T. Fukushima, T. Aida, T. Someya, *Science* **2008**, *321*, 1468.
- [38] W. C. J. Zuiderduin, C. Westzaan, J. Huetink, R. J. Gaymans, *Polymer* **2003**, *44*, 261.
- [39] S. Zulfiqar, M. Zulfiqar, M. Rizvi, A. Munir, *Polym. Degrad. Stab.* **1994**, *43*, 423.
- [40] L. F. Malmonge, L. H. C. Mattoso, *Polymer* **2000**, *41*, 8387.
- [41] M. A. Trunov, S. M. Umbrajkar, M. Schoenitz, J. T. Mang, E. L. Dreizin, *J. Phys. Chem. B* **2006**, *26*, 13094.
- [42] D. T. Osborne, M. L. Pantoya, *Combust. Sci. Technol.* **2007**, *179*, 1467.
- [43] M. L. Pantoya, S. W. Dean, *Thermochim. Acta* **2009**, *493*, 109.
- [44] B. D. Lee, R. Thiruvengadathan, S. Puttaswamy, B. M. Smith, K. Gangopadhyay, S. Gangopadhyay, S. Sengupta, *BMC Biotechnol.* **2013**, *13*, 30.
- [45] C. D. Yarrington, S. F. Son, T. J. Foley, *J. Propul. Power* **2010**, *26*, 734.
- [46] K. W. Watson, M. L. Pantoya, V. I. Levitas, *Combust. Flame* **2008**, *115*, 619.
- [47] J. Y. Ahn, J. H. Kim, J. M. Kim, D. W. Lee, J. K. Park, D. Lee, S. H. Kim, *Powder Technol.* **2013**, *241*, 67.
- [48] K. T. Sullivan, J. D. Kuntz, A. E. Gash, *J. Appl. Phys.* **2012**, *112*, 024316.
- [49] C. A. Crouse, C. J. Pierce, J. E. Spowart, *Combust. Flame* **2012**, *159*, 3199.